IEEE Access
Multidisciplinary | Rapid Review | Open Access Journal

Received October 20, 2019, accepted November 13, 2019, date of publication November 21, 2019, date of current version December 4, 2019.

Digital Object Identifier 10.1109/ACCESS.2019.2954914

Development of a 1-DOF Force Sensor Prototype Incorporating Tapered Fiber Bragg Grating for Microsurgical Instruments

ABDULFATAH A. G. ABUSHAGUR[1], NORHANA ARSAD[1], (Member, IEEE), MOHAMED M. ELGAUD[1,2], AND AHMAD ASHRIF A. BAKAR[1], (Senior Member, IEEE)

[1]Center of Advanced Electronic and Communication Engineering, Faculty of Engineering and Built Environment, Universiti Kebangsaan Malaysia, UKM Bangi, Selangor 43600, Malaysia
[2]College of Electrical and Electronics Technology (CEET), Benghazi 16063, Libya

Corresponding authors: Abdulfatah A. G. Abushagur (a.abushagur@gmail.com) and Ahmad Ashrif A. Bakar (ashrif@ukm.edu.my)

This work was supported in part by the Ministry of Energy, Science, Technology, Environment and Climate Change, under the grant scheme of Science fund under Grant 03-01-SF1317 and Grant DIP-2019-005.

ABSTRACT Decoupling between axial and transversal forces is an essential during tool-tissue interaction in many medicine surgeries; in particular where fine and precise manipulation is required to save the delicate tissues. One example of which is the vitreoretinal microsurgery (VRMS). When fiber Bragg grating based sensing technique is utilized, the cross-talk noise between the axial and transversal forces always show up severely due to its conventional wavelength shift method. To address the challenge, we have introduced theoretical method in which a combination of tapered FBG (TFBG) and bandwidth modulation method instead are used. Here in this paper, first phase of our ongoing progress to proof the concept and validate the simulation results is demonstrated experimentally. We have developed a prototype incorporated TFBG mimicking the structure of the ophthalmia's needle to measure temperature-insensitive 1-DOF axial forces. High speed plug and play (I-MON-256USB (Ibsen)) is used to monitor the reflection spectrum of the prototype sensor. An automated calibration system using LabVIEW with efficient algorithms have been developed to calculate and keep track the bandwidth variations as different values of axial forces applied. Calibration procedures are repeated three times to validate the consistency of the sensor response. Experimental results show that, the estimated force values of our prototype are consistent with their actual values with RMS error less than 0.356 N over the range (1N-10N), while temperature insensitivity is guaranteed.

INDEX TERMS Tapered FBG, FBG force sensing, tactile force sensor, vitreoretinal surgery, biomedical force sensor.

I. INTRODUCTION

Tapered fiber Bragg gratings (TFBG) are getting popular in the field of strain sensor as it responds differently to the strain and temperature [1], [2]. While its central wavelength shifts due to temperature variation as conventional FBG does, its spectral width can be tuned when tension force is applied longitudinally because of the variable cross-sectional area resulted from taper transition diameter. To this end, temperature-insensitive strain measurement is feasible. An additional advantage of TFBG is its tiny cross-sectional area, due to which a high sensitivity strain measurement is understandable.

Measuring 3-axis force components with very high sensitivity (sub-mN) in vitreoretinal surgeries is of interest of many researchers/ophthalmologists. An interesting research utilizing FBG sensing technique for VRMS application, through which several development stages have been carried out in [3]–[7] which led finally to highly sensitive 3-DOF instrument. Four standard FBG sensors have been integrated into customized ophthalmia's needle-hook, one inner FBG is fixed on its either side at the neutral axis of the needle with two intermediate tubes, while the other three FBG sensors have been attached onto the needle's surface. A force resolution of 0.25 mN was demonstrated in mentioned work

The associate editor coordinating the review of this manuscript and approving it for publication was Kin Kee Chow.

using wavelength shift interrogation method (WSIM). For more details on development stages can be found in [8]. An analogous presentation can be found in another medicine discipline [9]–[11], five FBG sensors configuration are interrogated also by WSIM, for development of a catheter device that able to measure a tri-axis distal contact forces in cardiac ablation procedures.

However, all the above-mentioned devices were unable to distinguish accurately between the axial and transversal forces which extracted at the tool-tip simultaneously. They relied on mechanical means to mitigate the effect of the cross-sensitivity of the WSIM. Our previous work in [12]–[14] have demonstrated theoretically that, the cross-talk noise caused by the simultaneous two forces can be decoupled completely. Our method is mainly combined both Bandwidth modulation method (BMM) and customized FBGs including TFBG technique. The former was to avoid the constantly wavelength shift method problem, while the latter enables us to encode the axial forces into its bandwidth due to its geometry. To proof the concept, ongoing needle-like prototyping is taking place in which three linear chirp FBGs together with inner TFBG will be integrated to achieve the desired noise-free 3-DOF force sensor. To this, TFBG as a first phase of this project is integrated in the inner cavity of the prototype shaft (at its neutral axis) to measure the axial forces is presented in this paper.

Bare fiber TFBG strain sensor has been extensively studied as bandwidth encoding strain-induced information [1], [15]–[17]. Due to its fragility (OD of cladding $= 40\mu$m), incorporating TFBG with an instrument is a challenge. To the best of found knowledge, for the first time in this paper we demonstrate an instrument incorporated TFBG force sensor, furthermore, capable to provide from constructed calibration curves consistent force measurement.

The paper is organized as follow, section II the mechanical structure of the developed prototype, section III the working and sensing principle of the device is explained, experimental setup and calibration procedure are explained in section IV, results and discussions and finally conclusion are discussed in section V and VI, respectively.

II. MECHANICAL STRUCTURE

Due to extremely small sizes of the actual instrument, and the lack of more advanced machinery techniques such as fiber laser, etc., the design of the instrument planned to pass through several successive stages of developments, for the current first stage, the developed prototype is made 10X bigger in size than the real vitreoretinal instrument.

The length of the shaft is approximately 30 mm, the outer and inner diameter respectively are 9 mm and 7.5 mm. To facilitate the procedure, the prototype is divided into three parts, middle, top and bottom hollow shafts as shown in Figure 1.The top and middle parts of the shaft are connected through linking shaft with an interference fit. The linking shaft is actually connecting the two parts together, and at the same time is an intermediate tube for the inner sensor to

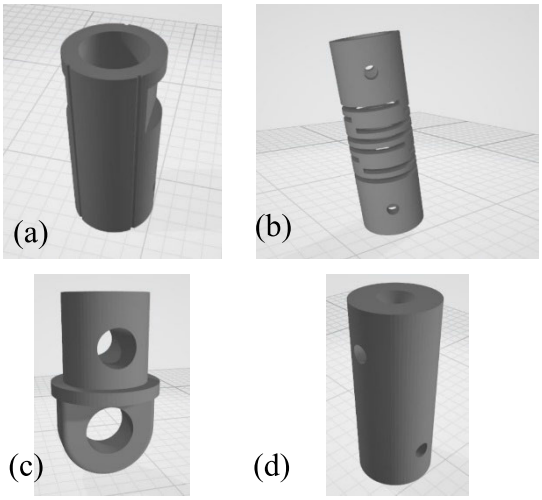

FIGURE 1. Prototype shaft structure, (a) the top part, (b) middle, (c) the bottom part (hook), and two pieces of (d) the top-middle and middle-bottom linking parts (intermediate tubes).

FIGURE 2. The assembled prototype using interference fit method.

be firmly fixed. The same connection has been established between the middle shaft and the lower part of the shaft which resembling ring or hook for hanging the weights during calibration process.

A. FLEXURE DESIGN (SPRING-LIKE)

For any metal in cylindrical shape, the shaft of the instrument is stiffer in axial than the transverse direction, and in order to amplify the axial sensor sensitivity several opening slots (flexure) are needed at which the TFBG supposed to be mounted.

Two parameters need to be considered when shaft flexure is made, torsion and transverse elasticity of the shaft. Both of them can affect the sensor functionality and instrument become vulnerable to break. Figure 2 shows the actual part after assembling the three parts of the shaft explained above.

B. INNER TFBG SENSOR ARRANGEMENT

Four FBGs are required to be incorporated into the prototype for 3-DOF force sensing. Two phases process will take place to mount the FBG's into their positions. The inner TFBG sensor is attached first for calibration in the current 1st phase. In the second phase, three linear chirped FBGs (LCFBG) will be embedded into grooves which are made onto the shaft surface.

The inner TFBG sensor is inserted axially at the neutral axis (see Figure 3) of the shaft, and with the help of two

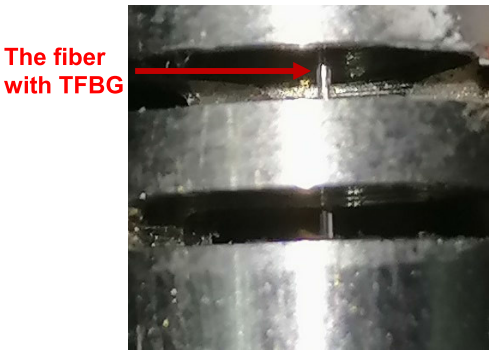

FIGURE 3. Preloaded inner TFBG which bonded on its either side within two intermediate tubes at the neutral axis after gluing process.

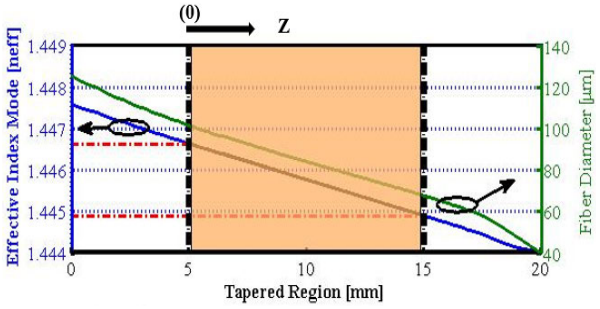

FIGURE 4. Tapered profile with the relative refractive indices and fiber diameter change.

intermediate tubes, both ends of the TFBG segment, the proximal and distal are bonded using an adhesive. Axial preload tension is applied to the TFBG sensor before the glue process, the bonding sites are shown in Figure 6.

To accomplish this, several packaging challenges are experienced which need to be considered in next design. Among that, the two intermediate tubes are hidden during fiber insertion and gluing process. The waist region of the tapered fiber is very fragile, thus any accidental bend the sensor becomes more prone to break, and the blind gluing due to hidden tubes doesn't help in controlling the amount of the glue needed. Furthermore, the dimensions of the beams between the slots require modification to meet the axial amplification of the design requirements.

III. TFBG WORKING AND SENSING PRINCIPLE

A. TFBG GEOMETRIC DESIGN

Unlike normal FBG, the TFBG is uniform gratings inscribed into a tapered region of a fiber. Tapered fiber can be fabricated by two methods, chemical and mechanical fusion. In our case the later method is considered in which the diameter of the fiber core also modified. As the core gets smaller, the boundary conditions of core-cladding will vary causes the effective refractive index (ERI) varies also and become localized following by that the local cross-sectional area along the down tapered profile. For the sake of explanation, Figure 4. illustrating the simulation results of the relation between the position of the grating and the numerically calculated effective refractive index and fiber diameter.

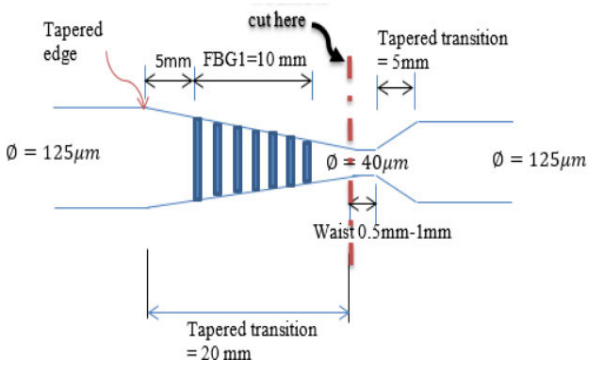

FIGURE 5. Tapered FBG schematic design.

It is seen that the grating extends between ≈1.4466 - 1.4449 of ERI as the fiber cladding diameter reduces from ≈ 101.2 μm to 67.5 μm. The various local ERI is the main reason of broadening the spectrum bandwidth of the TFBG; as the propagation constant of the fundamental mode varies with the fiber geometry. The difference between the local Bragg resonance wavelengths at the thinner and thicker section of the taper region determines the spectral width of the designed TFBG. Here in Figure 5, the whole fiber portion of the down and upper tapered region of the fiber containing the uniform gratings schematically is illustrated as designed. The gratings are written in the middle of the down taper transition region (TTR). The length of the segment sensor is 10 mm while the TTR is 20 mm. As shown the diameter of the cladding has been reduced from Φ125 μm to 40 μm. The red dashed line depicts the cutting position at which then bonded within the distal intermediate tube.

B. BANDWIDTH VS FORCE CALIBRATION

In this paper we first consider only the axial force measurement as encoded by the bandwidth of the TFBG sensor element. Due to the tapered and the rate change of the ERI along the grating length, the original bandwidth can be expressed as;

$$BW_{TFBG} = \lambda_B(L) - \lambda_B(0) = 2\Lambda\left[n_{eff}(L) - n_{eff}(0)\right] \quad (1)$$

Here $\lambda_B(0)$ and $\lambda_B(L)$ denotes the shorter and longer wavelengths of the TFBG sensor (see Figure 6), the Λ and n_{eff} are the grating period and ERI, respectively. According to Hook's law, strain induced by longitudinal push or pull can be found as;

$$\varepsilon_z = \frac{F_z}{EA} \quad (2)$$

Expression above expresses that; if the area of the object varies and not constant, the gradual strain is possible when axial forces are applied. Hence, as the calibration weights are applied axially to pull down the prototype, the flexure will respond to the action causing tension on the TFBG sensing segment. A nonuniform strain is then produced along the TFBG sensor consequently, which in turn allows the bandwidth to respond to the applied axial forces

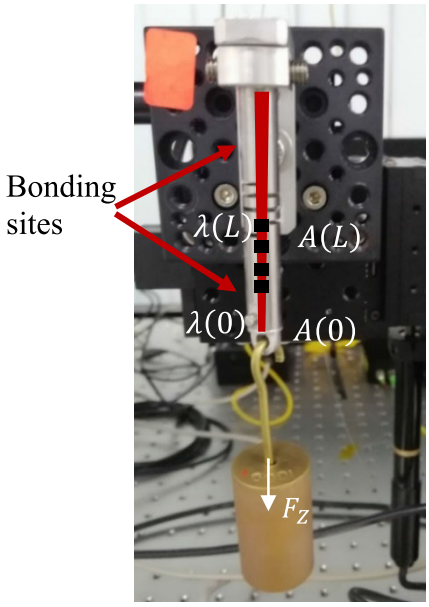

FIGURE 6. TFBG configuration inside the prototype.

($F_Z = weigths \times 9.81$) accordingly. The configuration of the inner TFBG inside the prototype is shown in Figure 6.It can be seen that the most extreme thin area will be elongated more than any elsewhere. Thus, the grating period will be elongated differently, each depends on the its local area, in other words, the gratings located at the thinnest part will be elongated more than the gratings at the thickest part at the other end of the TFBG due to the $\varepsilon_z(0) > \varepsilon_z(L)$.

Now notes that the shorter wavelength $\lambda(0)$(due to ERI) will shift to a greater extent compared to the longer one $\lambda(L)$. Thus, a reduction in the bandwidth should be observed. The fraction bandwidth is then negatively reacting to the axial force action as can be expressed as;

$$\Delta(BW_{TFBG}) = 2(1+\wp_e)\left[n_{eff}(L)\Lambda(L)\varepsilon_z(L) - n_{eff}(0)\Lambda(0)\varepsilon_z(0)\right] \quad (3)$$

Substituting the local strains in the equation above we get;

$$\Delta(BW_{TFBG}) = \frac{2(1+\wp_e)}{E}F_z\left[\frac{n_{eff}(L)\Lambda(L)}{A(L)} - \frac{n_{eff}(0)\Lambda(0)}{A(0)}\right] \quad (4)$$

Due to the small differences between the elasto-optic effects $\wp_e$ at both ends of the sensor, it is ignored here in the above expression. It is obvious that for every increase in an axial force, the more reduction in bandwidth will occur. This is attributed to the significant difference between the inverse of the cross-sectional areas $A(L) > A(0)$.

Thus, the measured signal of the effective spectral width variation is calculated by summing up the original bandwidth and the tuned fraction due to force applied;

$$\Delta BW_{eff}(\varepsilon_{ave}) = BW_{TFBG} + \Delta(BW_{TFBG}) \quad (5)$$

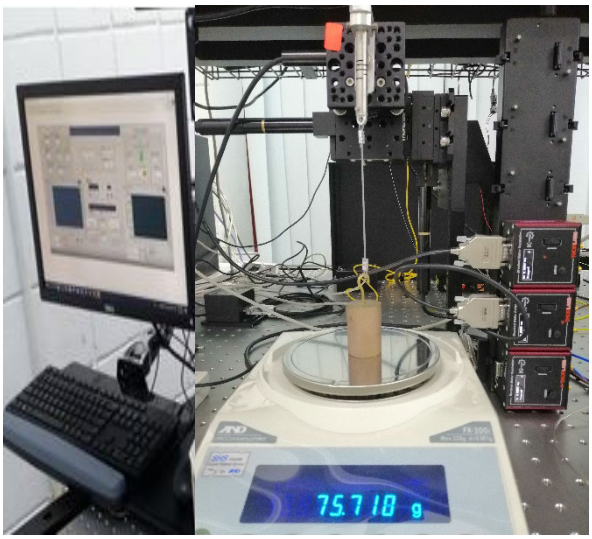

FIGURE 7. Picture shows the experimental setup (a) PC with LabVIEW running, (b) the setup.

And we get;

$$\Delta BW_{eff}(\varepsilon_{ave}) = BW_{TFBG} + \frac{2(1+\wp_e)}{E}F_z \times \left[\frac{n_{eff}(L)\Lambda(L)}{A(L)} - \frac{n_{eff}(0)\Lambda(0)}{A(0)}\right] \quad (6)$$

The difference between parameters inside the parenthesis and the multiplied constant can be expressed with the constant responsivity ratio k_ε. The axial force then can be measured as follow;

$$F_Z = \left|\frac{BW_{TFBG} - \Delta BW_{eff}(\varepsilon_{ave})}{k_\varepsilon}\right| \quad (7)$$

Here the coefficient k_ε defines the scale factor or responsivity ratio of the bandwidth-force relationship and can be determined from the calibration process.

IV. EXPERIMENTAL SETUP

The prototype force sensor element is calibrated with an automated system using the graphical software LABVIEW. Due to the size of the prototype, the resolution is quite small, thus the precision weighting scale is not used as it doesn't support weights greater than 300 grams, thus we rely on manual record for the forces applied. The results correspond to the forces are automatically recorded using the program. The real and schematic experimental set up are illustrated in Figure 7 and Figure 8, respectively.

Before starting to apply the load forces, the reference spectrum from the sensor is measured as shown in Figure 9.

The optical spectrum response of the I-MON-256USB is highly gaussian and assumes the FBGs also gaussian, thus if complicated shape like the current TFBG is used, the I-MON then would calculate wrongly the peak as a center wavelength. Furthermore, I-MON is not capable of measuring bandwidth of the signal, thus a new automated calibration system have been developed containing efficient algorithms to calculate the central wavelength and one for bandwidth

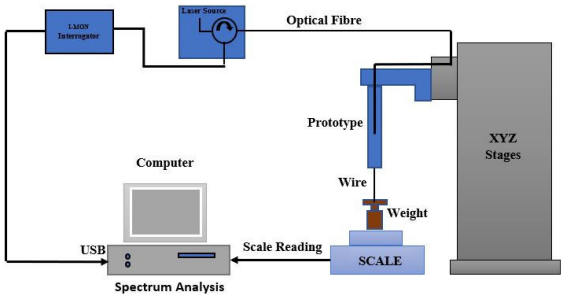

FIGURE 8. The complete schematic of the experimental setup for prototype instrument calibration process.

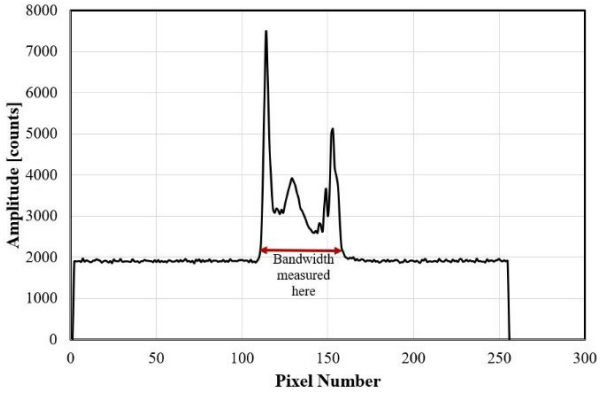

FIGURE 9. The spectrum as measured by center of gravity algorithm.

measurement with reasonable accuracy. The red arrow shows the position at which bandwidth is measured and observed during the calibration process. The x-axis here as shown in Figure 9 indicates the pixel number of the photodiode array detectors of the interrogator. It is worth mentioning, according to the I-MON design, the incident light of the longer wavelength impinges the lower pixel numbers. Calibration coefficients have been defined by I-MON designers to convert the pixels to the corresponding wavelengths, for which we used to calculate the bandwidth. Figure 10 depicts the same spectrum as a function of wavelengths after converting process.

The spectrum agrees with the theory which declaring that the peak of the shorter wavelengths of the TFBG is lower than the longer due to the power confined into the narrowed core with the diameter of the tapered region.

Unlike wavelength shift method, the cross-sensitivity due to the effect of both strain and temperature would be avoided by leveraging bandwidth interrogation method. The temperature change will only shift wavelength, so the whole spectrum shifts together maintain bandwidth unchanged due to the fact that, uneven temperature variation unlikely to happen within a small area. A temperature controller, relay, heat sink and heat element are used to control the temperature within the environment of the prototype sensor element as shown in Figure 11.

The calibration weights which are applied ranged from 100g-1000g which is then converted to the force magnitude

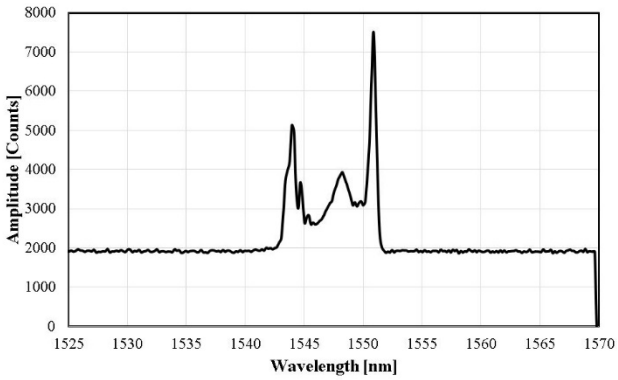

FIGURE 10. The spectrum as a function of wavelengths.

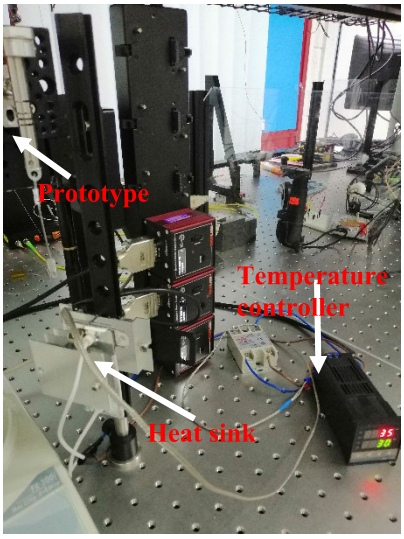

FIGURE 11. Controlling the temperature in the vicinity of the prototype.

(gravity magnitude is assumed 9.81 N/Kg). starting from 100 g with an increment of 100 g each step. The TFBG sensor response is sampled at 2 kHz rate using the FBG interrogator I-MON-256USB (from Ibsen). The prototype sensor is calibrated three times in sequence, each process the force applied starts from 100g and ended with 1000g in 100g incremental step. The calibration results are then utilized accordingly to map the sensor reading to the real time axial forces measurement.

V. RESULTS AND DISCUSSION

With regard to the equations expressed above, the nonuniform stretching of each localized grating pitch induced due to the axial forces will modify the local Bragg wavelength resonances. Furthermore, the area variability is the parameter which directly responsible for tuning the bandwidth as forces applied.

Spectrum width change due to axial force applied are shown in Figure 12. We only show the effect of three forces to show the bandwidth change clearly. As mentioned earlier there are three calibration procedures are carried out during the experiment at room temperature at 26°C.

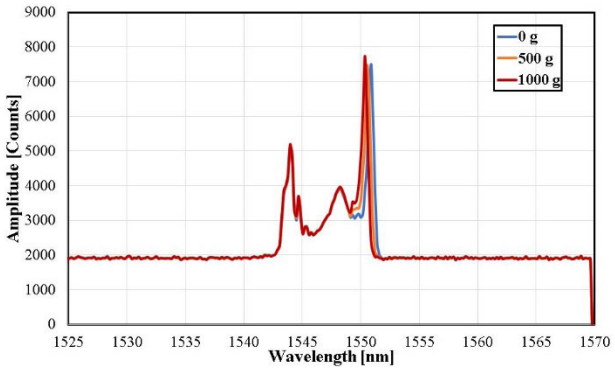

FIGURE 12. Spectrum width change due to axial force applied.

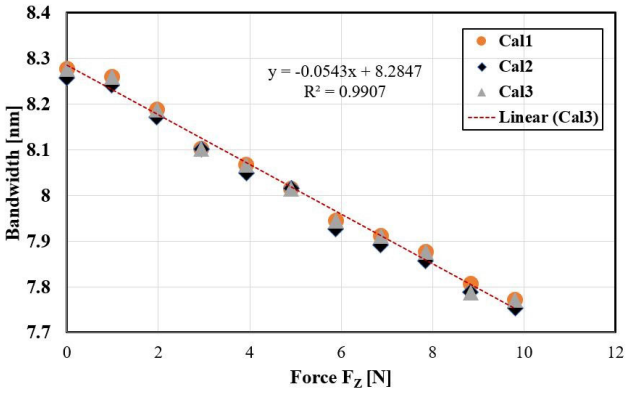

FIGURE 13. Bandwidth change as a function of axial force for the three calibration processes.

Figure 13 shows the linear relationship for all calibration processes. As the force increases the spectral width negatively response in linear pattern with a scale factor of responsivity ratio 54.3 pm/N. It is seen that from the Figure 13, although the sensor calibrations' results have shown quite consistency and agree with the theoretical models explained in previous sections, there are however for some values have shown up slight deviation, which we believe it could be attributed to the packaging and gluing process.

By determining the scale factor, we conduct a real time axial force measurement to evaluate our proof of concept prototype. The forces applied again are ranged from 100g to 1000g and the calculated force is recorded each step accordingly.

The mapping due to the calibration results using the linear fitting is depicted in Figure 14. It illustrates the calculated axial force as a function of the actual ones.

The linear fitting as can be seen shows slightly higher than one, and it passes through the origin. However, the trivial error and deviation can be observed, especially at 700g which depicting the highest error. Overall (RMS) error over the full scale of (1N-10N) is found to be <0.36 N, which is considered very promising result.

The main advantage of the bandwidth as a transducer, it remains essentially unaffected if no gradient strain introduced along the grating length, hence

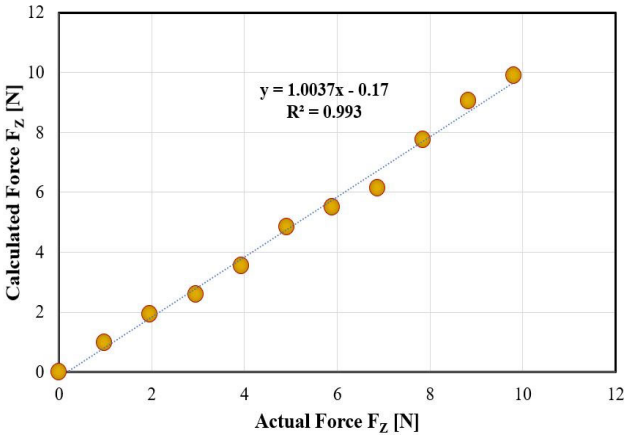

FIGURE 14. Calculated forces as compared with the actual forces.

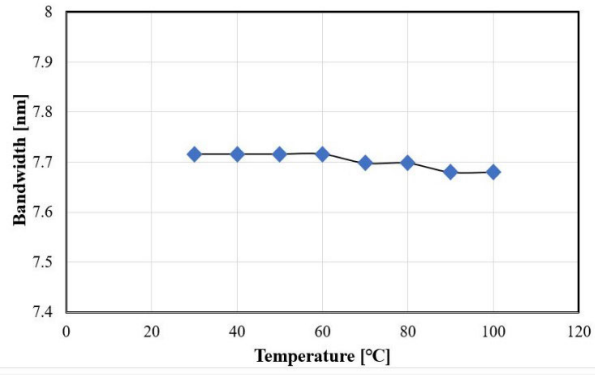

FIGURE 15. Bandwidth response to the environment temperature change in the vicinity of the prototype sensor (at static load of 1000g).

temperature-independent strain measurement guaranteed using TFBG. The temperature effect will be eliminated, and pure force measurement can be achieved. As unequal change in temperature within a short segment of the TFBG is unlikely to occur. The temperature impact is investigated using a controllable heat-element attached to a heat sink to control and change the environment vicinity around the sensor. Figure 15 shows the response of the bandwidth as the temperature in the vicinity of the sensor has been changed from 30 °C to 100 °C at static load of 1000 g.

As seen, there are two trivial reductions in the bandwidth response when the temperature exceeded 60°C and 80°C. This behavior is attributed to the glue's thermal expansion, where the small portion of the grating at $\lambda(0)$ might be implicitly glued inside the intermediate tube resulting in local elongation which in turn yields to bandwidth reduction. This is a good step forward in FBG sensing technique as the cross-sensitivity of the Bragg wavelength shift is limiting its implementation.

VI. CONCLUSION

Real time 3-axis force measurement is very vital in plenty of nowadays medicine disciplines. To this end, a first step of series developments towards tri-axial force measurements to

be used in vitreoretinal microsurgical procedures is demonstrated here experimentally. As proof of concept, we have developed a 1-DOF force sensing instrument prototype that encoding the axial force information in the spectral width of the TFBG sensor. We have started with the most challenges of the whole instrument design including the flexure structure and integrating the TFBG in the instrument. Our prototype demonstrated high degree of robustness in measuring the axial forces. With the aid of the I-MON interrogator device, real time force measurement sampled at even more 2kHz is feasible.

Extra degree of freedom force sensing by attaching three outer LCFBG sensors is currently in progress for measuring noise-free tri-axis force components.

REFERENCES

[1] T. Osuch, K. Markowski, and K. Jędrzejewski, "Fiber-optic strain sensors based on linearly chirped tapered fiber Bragg gratings with tailored intrinsic chirp," *IEEE Sensors J.*, vol. 16, no. 20, pp. 7508–7514, Oct. 2016.
[2] M. S. Bieda, P. Sobotka, and T. R. Woliński, "Chirped fiber Bragg grating written in highly birefringent fiber in simultaneous strain and temperature monitoring," *Appl. Opt.*, vol. 56, no. 6, pp. 1625–1630, Feb. 2017.
[3] I. Iordachita, "A sub-millimetric, 0.25 mN resolution fully integrated fiber-optic force-sensing tool for retinal microsurgery," *Int. J. Comput. Assist. Radiol. Surg.*, vol. 4, no. 4, pp. 383–390, 2009.
[4] X. He, P. Gehlbach, J. Handa, R. Taylor, and I. Iordachita, "Development of a miniaturized 3-DOF force sensing instrument for robotically assisted retinal microsurgery and preliminary results," in *Proc. 5th IEEE RAS EMBS Int. Conf. Biomed. Robot. Biomechatronics*, Aug. 2014, pp. 252–258.
[5] X. He, J. Handa, P. Gehlbach, R. Taylor, and I. Iordachita, "A sub-millimetric 3-DOF force sensing instrument with integrated fiber Bragg grating for retinal microsurgery," *IEEE Trans. Biomed. Eng.*, vol. 61, no. 2, pp. 522–534, Feb. 2014.
[6] B. Gonenc, A. Chamani, J. Handa, P. Gehlbach, R. H. Taylor, and I. Iordachita, "3-DOF force-sensing motorized micro-forceps for robot-assisted vitreoretinal surgery," *IEEE Sensors J.*, vol. 17, no. 11, pp. 3526–3541, Jun. 2017.
[7] B. Gonenc and I. Iordachita, "FBG-based transverse and axial force-sensing micro-forceps for retinal microsurgery," in *Proc. IEEE SENSORS*, Oct./Nov. 2017, pp. 1–3.
[8] A. A. G. Abushagur, N. Arsad, M. I. Reaz, A. Ashrif, and A. Bakar, "Advances in bio-tactile sensors for minimally invasive surgery using the fibre Bragg grating force sensor technique: A survey," *Sensors*, vol. 14, no. 4, pp. 6633–6665, 2014.
[9] T. Li, C. Shi, and H. Ren, "Three-dimensional catheter distal force sensing for cardiac ablation based on fiber Bragg grating," *IEEE/ASME Trans. Mechatronics*, vol. 23, no. 5, pp. 2316–2327, Oct. 2018.
[10] D. Shin, H.-U. Kim, and T. Kim, "Development and evaluation of tri-axial fiber Bragg grating in a measurement module for catheterization," in *Proc. 2nd Workshop Metrology Ind. 4.0 IoT (MetroInd4.0&IoT)*, Jun. 2019, pp. 158–161.
[11] T. Li, A. Pan, and H. Ren, "A high-resolution tri-axial catheter-tip force sensor with miniature flexure and suspended optical fibers," *IEEE Trans. Ind. Electron.*, to be published.
[12] A. A. G. Abushagur, A. A. A. Bakar, N. Arsad, and S. Shaari, "Sub-millinewton force sensor for Vitreoretinal microsurgery using linear chirp fiber Bragg grating," in *Proc. 5th Int. Conf. Photon. (ICP)*, Sep. 2014, pp. 41–43.
[13] A. A. G. Abushagur, A. A. A. Bakar, M. S. D. Zan, N. Arsad, and S. Shaari, "Decoupling method solving axial/transverse forces crosstalk in retinal microsurgery's force sensing instruments," in *Proc. 9th Int. Conf. Sensing Technol. (ICST)*, Dec. 2015, pp. 295–299.
[14] A. A. G. Abushagur, A. A. A. Bakar, M. S. D. B. Zan, and N. Arsad, "A novel technique employing tapered fiber Bragg grating to solve the axial/transverse forces crosstalk in microsurgical instruments," *IEEE Sensors J.*, vol. 16, no. 21, pp. 7671–7680, Nov. 2016.
[15] T. Osuch, "Tapered and linearly chirped fiber Bragg gratings with co-directional and counter-directional resultant chirps," *Opt. Commun.*, vol. 366, pp. 194–199, May 2016.
[16] K. Markowski, K. Jedrzejewski, and T. Osuch, "Numerical analysis of double chirp effect in tapered and linearly chirped fiber Bragg gratings," *Appl. Opt.*, vol. 55, no. 17, pp. 4505–4513, Jun. 2016.
[17] T. Osuch, K. Markowski, and K. Jędrzejewski, "Numerical model of tapered fiber Bragg gratings for comprehensive analysis and optimization of their sensing and strain-induced tunable dispersion properties," *Appl. Opt.*, vol. 54, no. 17, pp. 5525–5533, Jun. 2015.

ABDULFATAH A. G. ABUSHAGUR received the bachelor's degree in electrical and electronics engineering from Universiti Tenaga Nasional, in 2002, the master's degree in communications and network system engineering from Universiti Putra Malaysia, in 2004, and the Ph.D. degree in electrical engineering from The University of Queensland, Australia, in 2010. He is currently an Associate Professor with the Center of Advanced Electronic and Communication Engineering, Faculty of Engineering and Built Environment, Universiti Kebangsaan Malaysia, involving in teaching, research and industrial consultation. He is actively involved in the Institution of Electrical and Electronics Engineers (IEEE), the Optical Society of America, and the Fiber Optic Association Inc., USA. He is devoting his research work on optical sensors in environmental and biomedical application, specifically in optical techniques of surface plasmon resonance, material coated optical fiber, and optical feedback interferometry.

NORHANA ARSAD (M'10) received the B.Eng. degree in computer and communication systems and the M.Sc. degree in photonics from Universiti Putra Malaysia (UPM), Malaysia, in 2000 and 2003, respectively, and the Ph.D. degree from the University of Strathclyde, Glasgow, U.K., in 2010. She is currently an Associate Professor with the Center of Advanced Electronic and Communication Engineering, Faculty of Engineering and Built Environment, Universiti Kebangsaan Malaysia. Her research interests are in the investigation and design of fibre laser systems for application in spectroscopy, gas sensing, and photonics technology.

MOHAMED M. ELGAUD received the B.E. degree in electrical and electronic engineering from Benghazi University, Benghazi, Libya, in 2005, and the master's and Ph.D. degrees in electrical, electronic engineering from Universiti Kebangsaan Malaysia, in 2011 and 2019, respectively. His research interest is in signal processing methods to improve the performance of time domain multiplexed FBG sensor arrays.

AHMAD ASHRIF A. BAKAR received the B.E. degree in electrical engineering from the Higher Institute of Mechanical, Electrical Engineering, Hun, Libya, and the master's and Ph.D. degrees from Universiti Kebangsaan Malaysia (UKM), Malaysia, in 2013 and 2018, respectively. During his Ph.D. study, he proposed a novel method using tapered fiber Bragg grating sensors to improve the performance of microsurgical force sensor.

He is currently working as a Research fellow at the Center of Advanced Electronic and Communication Engineering, Faculty of Engineering and Built Environment, UKM. At the same time, he is currently working as a Research Fellow at the Computing and Informatics Faculty, Multimedia University (MMU). His research interests include optical fiber sensing and its application, medical instruments, structure health monitoring, and hybrid SDN networking measurement.